

# Deep Learning for Printed Mottle Defect Grading \*

Jianhang Chen<sup>1</sup>, Qian Lin<sup>2</sup>, Jan P. Allebach<sup>1</sup>;

<sup>1</sup>School of Electrical and Computer Engineering, Purdue University; West Lafayette, Indiana, USA

<sup>2</sup>HP Labs, HP Inc; Palo Alto, California, USA

## Abstract

In this paper, we propose a new method for printed mottle defect grading. By training the data scanned from printed images, our deep learning method based on a Convolutional Neural Network (CNN) can classify various images with different mottle defect levels. Different from traditional methods to extract the image features, our method utilizes a CNN for the first time to extract the features automatically without manual feature design. Different data augmentation methods such as rotation, flip, zoom, and shift are also applied to the original dataset. The final network is trained by transfer learning using the ResNet-34 network pre-trained on the ImageNet dataset connected with fully connected layers. The experimental results show that our approach leads to a 13.16% error rate in the T dataset, which is a dataset with a single image content, and a 20.73% error rate in a combined dataset with different contents.

## Introduction

Printed defects such as mottle, banding, drips, drop-density-differences, ghosting, folds, streaks, and smudges commonly appear on printed images. Visual inspection is the primary approach to evaluating defect conditions. According to [1], there are two different methods for an operator to inspect the defects. First, an operator is fully occupied with one machine when the prints come off the press. Second, an operator could check a stack of prints instead. Thus, the operator does not need to wait; but paper is wasted. However, human-based defect inspection is limited to qualitative evaluation only, and is time-consuming. Since automated defect detection can address the limitations of human-based inspection, many researchers and companies have been attracted to the development of computer vision-based method for defects grading and detection [2, 3, 4, 5].

Mottle is a printed defect caused by low-frequency random non-uniformity. The mottle defect is different from banding or any other periodic non-uniform defect that could appear at any gray level or any color. Figure 1 shows an example where the printed image quality is severely degraded by the mottle defect in certain areas. From the perspective of human visual perception, the spatial frequency, size, contrast, sharpness, illumination, and viewing distance can affect the perception of the mottle defect. Figure 2 provides two visual examples of mottle defects, which are zoomed in views from Figure 1.

In this paper, we categorize the mottle defect level into 4 classes based on the defect degree:

1. Class A means the printed image is visually good. The uniform areas in the printed image look highly smooth and uniform.

\*Research supported by HP Labs, Inc., Palo Alto, CA 94304.



Figure 1. A printed image with mottle defect.

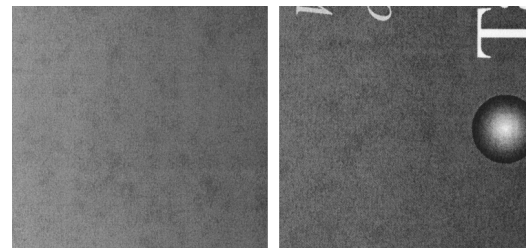


Figure 2. Zoomed in views of the mottle defect. The left image has lower density with uniform content. The right image has higher density with non-uniform content.

2. Class B means the printed image is visually sufficient. There are some non-uniform blotches in the printed image.
3. Class C means a lack of printed image quality. There are some large non-uniform blotches in the image.
4. Class D means the printed image quality is very poor. There are very large non-uniform blotches.

## Previous Work on PQ Defect Assessment

Early work on print quality (PQ) defect diagnosis reported a tool for computing the strengths of various PQ defects from scanned pages, based on procedures recommended by an ISO standard [6]. Tools to enable the customer to troubleshoot his or her print quality (PQ) issues by visual inspection were also developed. This work consisted of PQ troubleshooting pages [7], web-based troubleshooting tools [8], and tools for simulating the appearance of print quality defects on test pages [9]. For banding, in particular, tools were developed to model the defect and measure its strength via psychophysical experiments [10, 11, 12, 13], as well as to estimate the period of periodic

banding defects [14, 15, 16]. Some efforts focused on wavelets as a tool for PQ analysis [17, 18, 19]. Later efforts considered the visibility of PQ defects in the presence of customer content [5, 2, 1, 20, 21, 22, 23, 24, 3, 25] and the identification of specific defects, such as mottle [52, 26, 27, 28, 29, 30], macro-uniformity [31], fading [32, 33], ghosting [34], local nonuniformities [35, 36, 37], and streaks [38, 39]. Other efforts considered a more comprehensive set of PQ defects [53, 40, 41, 42]. More recently, machine learning approaches (linear regression and support vector regression) have been deployed to predict the visibility of PQ defects based on ground truth provided by human observers [31, 43], including the image quality ruler method [44, 19, 45, 46]. The most recent efforts have included the development of a comprehensive system for assessing a variety of PQ defects in customer content [47], including segmentation of the page into multiple regions of interest, according to the type of page content [48]. During the entire course of this time, a number of standards have been developed for assessing PQ [49, 50, 51].

In the ISO/IEC 24790 international standard [50], which is a revised version of ISO/IEC 13660 [51], a method for hardcopy image quality is introduced which uses a single high-pass filter that integrates many components in an area to a value. In this method, the standard deviation of  $2mm \times 2mm$  cells for an area larger than  $20mm \times 20mm$  is calculated. This method is useful for qualitative comparison. In another paper [52], the tile method is modified and expanded to provide more discrete data including different cell sizes, the average of density, standard deviation, the average of standard deviation and the standard deviation of standard deviation, which can be used for quantitative analysis for the mottle defect. Other traditional methods [52, 53] use the information of cluster, statistics, and wavelets for the mottle defect characterization problem. Traditional computer vision methods estimate the mottle defect by extracting visual features, such as frequency and standard deviation, from the image and characterize the defect level using a threshold based on experimental results. The main drawback of those approaches is that they need manually designed features for the printed defects.

### Deep Convolutional Neural Networks

In recent years, the deep Convolutional Neural Network (CNN) has become one of the most efficient methods to solve many computer vision problems, such as segmentation [54, 55], detection [56], tracking [57], and pose estimation [58, 59]. With annotated data, the deep learning based-approach can treat the computer vision problem as a regression or classification task by extracting features in the CNN layers and joining them in fully connected layers. In contrast to the aforementioned traditional methods, the deep neural network can be trained in an end-to-end manner based on the dataset without the necessity to manually design features and thresholds.

In most traditional methods, the mottle defect level depends on the local areas in an image with uniform color or grayscale. In the deep learning approach, the entire image can be used as the input to the network. The deep neural networks work on printed images with different and non-uniform contents. The traditional feature-based methods are limited to a specific defect. However, deep learning methods can easily be extended to different types of printed defects by training on different datasets.

In this paper, we propose a deep learning-based method for

printed mottle defect grading. We collected the training data scanned from printed pages and trained a ResNet-34 model to classify various images with different mottle defect levels.

### Dataset

In this paper, we present two new datasets used for mottle defect grading in printed pages. The first dataset is named the T dataset with 135 images with different levels of the mottle defect, as shown in Figure 3. In the T dataset, there are 22 images in class A, 63 images in class B, 45 images in class C, and 5 images in class D. All the images in the T dataset have the same “textile” content. The second dataset is named the M dataset with 145 images as shown in Figure 4. In the M dataset, there are 87 images in class A, 42 images in class B, 15 images in class C, and 1 image in class D. The images in the M dataset have different contents. All images in the two datasets are grayscale and have been annotated by professional operators. Here, the classes denote different quality levels ranging from the highest (A) to the lowest (D).



Figure 3. Examples from the T dataset which has 135 images with the same “textile” content.

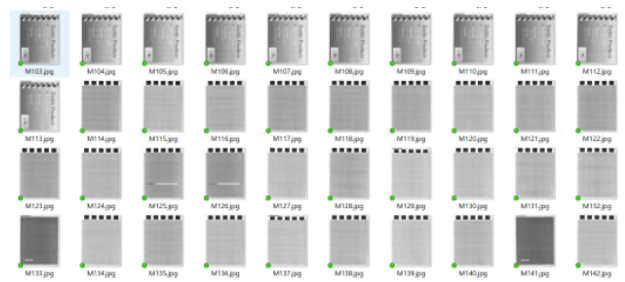


Figure 4. Examples from the M dataset which has 145 images with different contents.

### Data Augmentation and Unbalanced Datasets

The deep learning-based methods require a large amount of training data. To increase the dataset size in our work, we apply different data augmentation methods such as rotation, flip, zoom, and shift, as shown in Figure 5. Some commonly used filters, such as the Gabor filter, and Gaussian filter that were used for augmentation of the ImageNet Dataset [60] are not used in this work because the filters might change the feature distribution of the mottle defects.



**Figure 5.** Examples of data augmentation: a combination of augmentation methods such as rotation, flip, zoom, and shift are used in the above images.

In both the T dataset and the M dataset, there are fewer samples in the D class, which corresponds to the poorest printed image quality. An unbalanced dataset like this may cause poor classification accuracy. Several methods have been developed to increase the number of data for the classes with fewer samples. The first method uses a simulation method to generate synthetic data. It requires an accurate simulation model of the printing process and the mottle defect generation process, which are not available in our case. The second method randomly under-samples images from the original dataset. A higher sampling probability is assigned to the class with fewer samples to achieve balance. Although it is easy to implement, the under-sampling process gets rid of some samples and loses important information in the original dataset. The third method randomly over-samples images from the classes with insufficient samples. The maximum number of duplicates is limited to avoid overfitting in the training dataset.

In this work, the images in classes with insufficient data are over-sampled; and the maximum number of duplicates is limited to 15. Then, the data augmentation is implemented for the training dataset. In the final dataset, the T dataset has 192 images with 44 images in class A, 63 images in class B, 45 images in class C, and 40 images in class D. The augmented T dataset is divided into a training set with 154 images and a validation set with 38 images. The T dataset and the M dataset are merged to generate the combined dataset. After augmentation, the combined dataset has 410 images with different contents. There are 109 images in class A, 105 images in class B, 106 images in class C, and 90 images in class D. The augmented combined dataset has 328 images in the training set and 82 images in the validation set. The resolution of all images is  $5100 \times 6600$  (600 DPI).

## Network and Training Process

The ResNet-34 [61] network is used as a feature extraction backbone. The ResNet-34 structure has several residual blocks, as shown in Figure 8. The feature extraction network is followed by fully connected layers. In the regression network, the

last layer has a single output, as shown in Figure 6. The four classes [A,B,C,D] are mapped to scores [0,1,2,3]. In the classification task, the last fully connected layer has four outputs, as shown in Figure 7. The final network is trained by transfer learning using ResNet-34 pre-trained on ImageNet [60] connected with fully connected layers. In the first step, the ResNet-34 convolution layers are frozen. Second, the fully connected layers are trained with a specified learning rate. Third, the convolution layers are unfrozen and the whole network is retrained with a lower learning rate. In the training process, the loss function is MSE Loss adding dropout regularization loss for the regression task, and cross-entropy loss adding dropout regularization loss for the classification task. In the validation/testing stage, the dropout regularization loss is turned off.

To find the best learning rate for training, in each epoch, stochastic gradient descent is trained with a lower learning rate first. Then the learning rate is multiplied by a factor in each mini-batch until a higher learning rate is reached. We record the loss in each iteration for different learning rates and choose the learning rate with a relatively lower loss. The triangular learning rate policy [62] is used in the training stage. The learning rate value changes between the minimal and maximal learning rates. The increase of the learning rate will force the network model to explore a new parameter space when the loss function decreases slowly or stops decreasing.

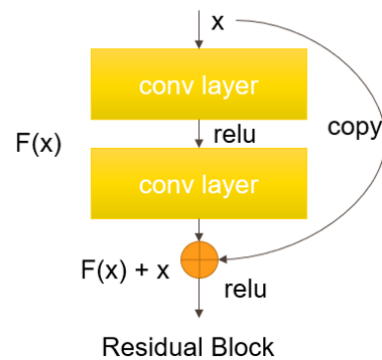


**Figure 8.** Structure of residual block.

## Experimental Result

In this work, the deep CNN is trained on two different datasets. Three experiments are trained on the augmented T dataset and the other two experiments are trained on the augmented combined dataset. In the first experiments, we train the dataset using cropped input images and combine the results of the small patches to generate the final prediction. We treat the defect grading problem as a regression or a classification problem to explore the effect on the prediction accuracy. In the last two experiments, the combined dataset is used to further prove that the network can be generalized to mottle defect grading with different contents.

### Prediction Using Cropped Patches

In the first experiment, the original input image in the T dataset is cropped to  $600 \times 600$  resolution patches without overlap. The whole T dataset is cropped into 11880 patches in four classes: [A :  $22 \times 88$ , B :  $63 \times 88$ , C :  $45 \times 88$ , D :  $5 \times 88$ ]. The

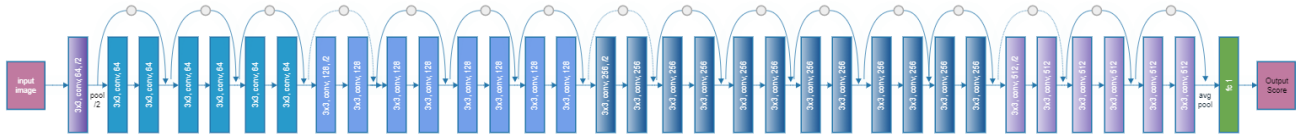


Figure 6. Network structure for mottle defect regression task.



Figure 7. Network structure for mottle defect classification task.

training set has 9504 images and the validation set has 2376 images, respectively. The error rate on the training set is 38.55%. The confusion matrix is shown in Figure 9.

**Mottle Grading Regression and Classification on T dataset**

The second and third experiments are performed on the T dataset. In the regression task, the input is resized to 1000 × 1000 resolution and the output is a single score mapped to four classes [A, B, C, D]. We first use the learning rate finding as shown in Figure 11, which suggests a learning rate of 2e-2. Then we freeze the convolutional layers, unfreeze the fully connected layers, and train for 40 epochs. Finally, we unfreeze all layers and train with a lower learning rate in the range [3e-5, 2e-2] for 5 epochs. The batch size is 16 in the training process. Figure 12 shows the loss in the training and validation sets. The best root mean squared error for regression is 0.45, as shown in Figure 13. The final error rate is 21.05%.

	A	B	C	D
Actual A	467	46	15	0
Actual B	321	363	351	21
Actual C	25	103	549	27
Actual D	0	0	7	81

Figure 9. Confusion matrix for prediction using cropped patches. The x-axis is the prediction of the networks and the y-axis is the ground truth of the data.

In the prediction stage, the original image is cropped to 88 patches as shown in Figure 10. The 88 patches are fed to the convolutional neural network to output a 88 dimension score vector. The final prediction is generated by averaging or majority voting over the score vector. On the validation set, the error rate is 33.33% by the average score method and 37.04% by the majority voting method. The result shows that the accuracy of using local cropped patches is not satisfactory.

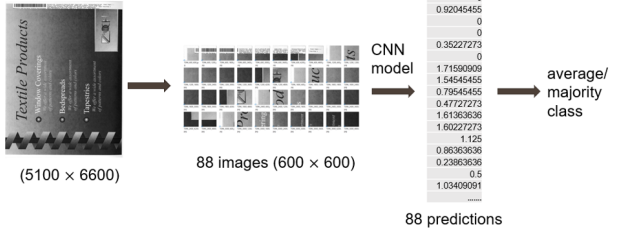


Figure 10. Defect prediction using cropped patches.

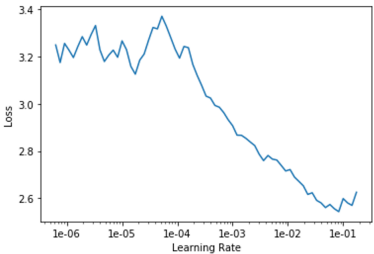
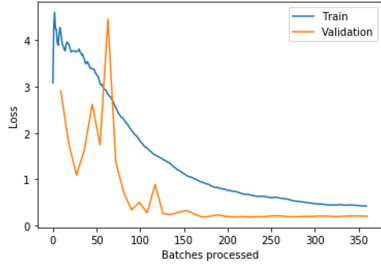
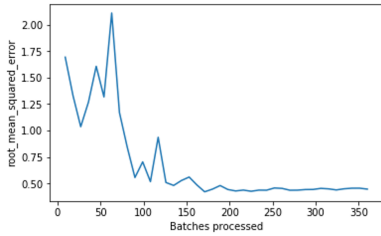


Figure 11. Finding the learning rate for the regression method on the T Dataset.



**Figure 12.** Loss for regression on the T training and validation sets. The dropout rate in the training stage is 50%. The loss in the training stage is calculated by adding MSE loss and the dropout regularization loss of the weights. The loss in the validation stage is MSE loss only.



**Figure 13.** Root mean squared error for regression on the T dataset.

In the classification task, the last fully connected layer has four outputs indicating four classes. The loss for the classification task is shown in Figure 14. The confusion matrix is shown in Figure 15. The error rate is 13.16%, which is better than the regression task in the T dataset with the “textile” content images.

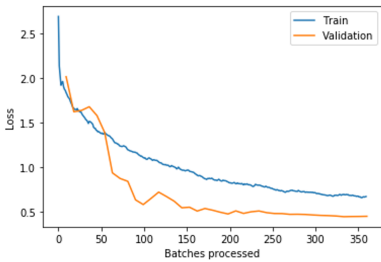


**Figure 14.** Loss for classification in the T training and validation sets. The dropout rate in the training stage is 50%. The loss in the training stage is calculated by adding cross-entropy loss and the dropout regularization loss of the weights. The loss in the validation stage is cross-entropy loss only.

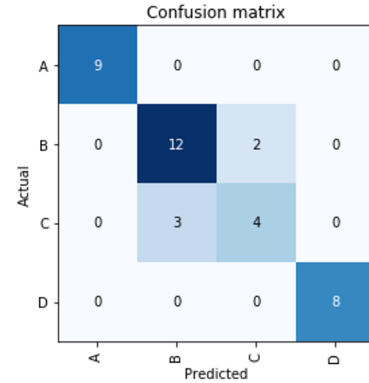


**Figure 15.** Confusion matrix for classification on the T dataset. The x-axis is the prediction of the network, and the y-axis is the ground truth of the data.

### Mottle Grading Regression and Classification on the Combined Dataset

The second and third experiments are performed on the combined dataset. Mottle grading regression and classification on the combined dataset have a setting similar to that of the tasks on the T dataset. The combined dataset is more challenging, since it has a large variety of image contents. In the regression task, Figure 16 shows the loss in the training and validation sets. The best root mean squared error for regression is 0.49 as shown in Figure 17. The final error rate is 21.95%. In the classification task, the loss for classification is shown in Figure 18. The confusion matrix is shown in Figure 19. The best error rate is 20.73% which is similar to the regression task.

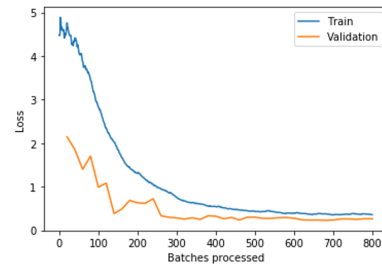


**Figure 16.** Loss for regression in the combined training and validation sets. The dropout rate in the training stage is 50%. The loss in the training stage is calculated by adding MSE loss and the dropout regularization loss of the weights. The loss in the validation stage is MSE loss only.

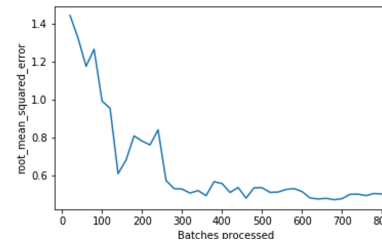


**Figure 17.** Root mean squared error for regression on the combined dataset.

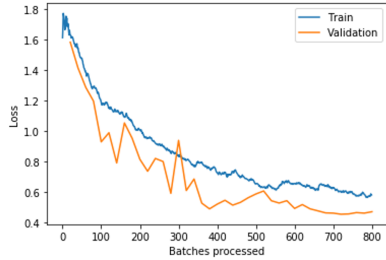


**Figure 18.** Loss for classification in the combined training and validation sets. The dropout rate in the training stage is 50%. The loss in the training stage is calculated by adding cross-entropy loss and the dropout regularization loss of the weights. The loss in the validation stage is cross-entropy loss only.

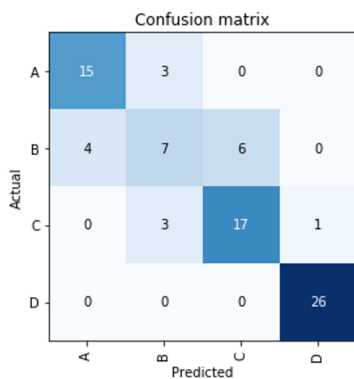


**Figure 19.** Confusion matrix for classification on combined dataset. The x-axis is the prediction of the network, and the y-axis is the ground truth of the data.

## Conclusion

In this paper, we propose a new deep learning-based method for printed mottle defect grading. Different from traditional methods such as feature extraction using  $\Delta E$  variation, our method utilizes a CNN for the first time to extract the feature automatically by stochastic gradient descent. Transfer learning and data augmentation methods are used to train a robust mottle defect grader. The proposed deep learning mottle characterization method can be used in mottle grading not only for the test image with the same uniform content as seen in the training set but for printed images with different contents. The mottle grading method achieves a 13.16% error rate in the T dataset with the same content and a 20.73% error rate in the combined dataset with different contents. The proposed method can also be generalized to other printed defects, such as streaks given an annotated streak dataset.

## Acknowledgment

The authors would like to thank Ren-San Wang from HP Shanghai for providing the mottle assessment dataset.

## References

[1] M. Vans, S. Schein, C. Staelin, P. Kisilev, S. J. Simske, R. Dagan, and S. Harush, "Automatic Visual Inspection and Defect Detection on Variable Data Prints," *Journal of Electronic Imaging*, 20(1), 013010 (2011)

[2] P. Kisilev, and G. Ruckenstein, "Print Defect Detection," U.S. Patent no. 7,519,222, (2009)

[3] Y. Wang, S. Xu, Z. Zhu, Y. Sun, and Z. Zhang, "Real-time Defect Detection Method for Printed Images Based on Grayscale and Gradient Differences," *Journal of Engineering Science & Technology Review*, 11.1, (2018)

[4] J. Lundström, and A. Verikas, "Assessing Print Quality by Machine in Offset Colour Printing," *Knowledge-Based Systems*, pages 70-79, (2013)

[5] N. G. Shankar, N. Ravi, and Z. W. Zhong, "On-Line Defect Detection in Web Offset Printing," in *Proceedings of 4th International Conference on Control and Automation*, (2003)

[6] J. Grice and J. P. Allebach, "The Print Quality Toolkit: An Integrated Print-Quality Assessment Tool," *Journal of Imaging Science and Technology*, vol. 43, pp. 187-199, (1999)

[7] W. Jang, M. C. Chen, J. P. Allebach, and G. T. C. Chiu, "Print Quality Test Page," *Journal of Imaging Science and Technology*, vol. 48, pp. 432-446, (2004)

[8] H. Santos, H. J. Park, R. Kumontoy, K. Low, M. Ortiz, C. W. Kim, P. Choe, S. Leman, K. Oldenburger, M. Lehto, X. Lehto, and J. P. Allebach, "A Web-based Self-diagnosis Tool to Solve Print Quality Issues," *Journal of Imaging Science and Technology*, vol. 54, no. 4, pp. 040503-1 – 040503-13, (2010)

[9] W. Jang and J. P. Allebach, "Simulation of Print Quality Defects," *Journal of Imaging Science and Technology*, vol. 49, pp. 1-18, (2005)

[10] Y. Bang, Z. Pizlo, and J. P. Allebach, "Banding Assessment with Controlled Halftoning: The Ten Printer Experiment," *Journal of Imaging Science and Technology*, vol. 50, no. 6, pp. 522-529, (2006)

[11] O. Arslan, Z. Pizlo, and J. P. Allebach, "Softcopy Banding Visibility Assessment," *Journal of Imaging Science and Technology*, vol. 51, no. 3, pp. 271-281, (2007)

[12] B. Min, Z. Pizlo, and J. P. Allebach, "Development of Softcopy Environment for Primary Color Banding Visibility," in *Image Quality and System Performance V*, SPIE, vol. 6808, (2008)

[13] T. Ha, J. P. Allebach, and D. Cha, "Measurement and Analysis of Banding Artifacts in Color Electrophotographic Printers," in *Proceedings NIP24: IS&T's 24th International Conference on Digital Printing Technologies*, (2008)

[14] J. Zhang, S. Astling, R. Jessome, E. Maggard, T. Nelson, M. Q. Shaw, and J. P. Allebach, "Assessment of Presence of Isolated Periodic and Aperiodic Bands in Laser Electrophotographic Printer Output," in *Image Quality and System Performance X*, SPIE vol. 8653, (2013)

[15] J. Zhang and J. P. Allebach, "Estimation of Repetitive Interval of Periodic Bands in Laser Electrophotographic Printer Output," in *Image Quality and System Performance XII*, SPIE vol. 9396, (2015)

[16] W-E. Huang, E. Maggard, R. Jessome, Y. Bang, M. Choi, and J. Allebach, "Cost-Function-Based Repetitive Interval Estimation Method with Synthetic Missing Bands for Periodic Bands in Electrophotographic Printer," in *Image Quality and System Performance XVI*, IS&T Electronic Imaging, (2019)

[17] K. Donohue, C. Cui, and M. V. Venkatesh, "Wavelet analysis of print defects," in *IS&T's 2002 PICS Conference*, pp. 42-47, (2002)

[18] A. Eid, B. Cooper, and E. Rippetoe, "A Unified Framework for Physical Print Quality," in *Image Quality and System Performance IV*, SPIE-IS&T Electronic Imaging, vol. 6494, p. 64940C, (2007)

[19] X. Liu, G. Overall, T. Riggs, R. Silveston-Keith, J. Whitney, G. T. C. Chiu, and J. P. Allebach, "Wavelet-Based Figure of Merit for Macrouniformity," in *Image Quality and System Performance X*,

- SPIE vol. 8653, (2013)
- [20] S. Hu, H. Nachlieli, D. Shaked, S. Shiffman, and J. P. Allebach, "Color-Dependent Banding Characterization and Simulation on Natural Document Images," in *Color Imaging XVII: Displaying, Processing, Hardcopy, and Applications*, SPIE vol. 8292, (2012)
- [21] X. Jing, H. Nachlieli, D. Shaked, S. Shiffman, and J. P. Allebach, "Masking Mediated Print Defect Visibility Predictor," in *Image Quality and System Performance IX*, SPIE vol. 8293, (2012)
- [22] J. Zhang, H. Nachlieli, D. Shaked, S. Shiffman, and J. P. Allebach, "Psychophysical Evaluation of Banding Visibility in the Presence of Print Content," in *Image Quality and System Performance IX*, SPIE vol. 8293, (2012)
- [23] Y. Liu and J. P. Allebach, "A Computational Texture Masking Model for Natural Images Based on Adjacent Visual Channel Inhibition," *Image Quality and System Performance XI*, SPIE vol. 9016, (2014)
- [24] Y. Liu and J. P. Allebach, "A Perceptual Masking Model for Natural Images with Additive Defects and Detail Loss, Based on Adjacent Visual Channel Inhibition," in *Human Vision and Electronic Imaging XX*, SPIE vol. 9394, (2015)
- [25] Z. Xiao, S. Xu, E. Maggard, M. Shaw, K. Morse, and J. Allebach, "Detection of Color Fading in Printed Customer Content," in *Color Imaging XXIII: Displaying, Processing, Hardcopy, and Applications*, IS&T Electronic Imaging, (2018)
- [26] P. Johansson, "Print Mottle Evaluation by Band-pass Image Analysis," *Advances in Printing Science and Technology*, Vol 22, pp. 403-412, (1994)
- [27] R. Rosenberger and D. Clark, "Stochastic Frequency Distribution Analysis as Applied to Ink Jet Print Mottle Measurement," in *Proceeding of IS&T's 17th Non-Impact Printing Conference*, pp. 808-812, (2001)
- [28] C. Fahlcrantz, P. Johansson, and P. Åslund, "The Influence of Mean Reflectance on Perceived Print Mottle," *Journal of imaging Science and Technology*, vol. 47, no. 1, pp. 54-59, (2003)
- [29] A. H. Eid, B. E. Cooper, and E. E. Rippetoe, "Characterization of Mottle and Low Frequency Print Defects," in *Image Quality and System Performance V*, SPIE vol. 6808, (2008)
- [30] S. Khullar, E. Saber, S. Dianat, J. Trask, R. Lawton, and M. Shaw, "Automatic Multi-resolution Spatio-frequency Analysis for Print Mottle Evaluation," in *Color and Imaging Conference*, vol. 2009, no. 1, pp. 95-100, (2009)
- [31] M. Q. Nguyen, S. Astling, R. Jessome, E. Maggard, T. Nelson, M. Q. Shaw, and J. P. Allebach, "Perceptual Metrics and Visualization Tools for Evaluation of Page Uniformity," in *Image Quality and System Performance XI*, SPIE vol. 9016, (2014)
- [32] N. Yan, E. Maggard, R. Fothergill, R. J. Jessome, and J. P. Allebach, "Autonomous Detection of ISO Fade Point with Color Laser Printers," in *Image Quality and System Performance XII*, SPIE vol. 9396, (2015)
- [33] Y. Ju, E. Maggard, R. J. Jessome, and J. P. Allebach, "Autonomous Detection of Text Fade Point with Color Laser Printers," in *Image Quality and System Performance XII*, SPIE vol. 9396, (2015)
- [34] X. Jing, S. Astling, R. Jessome, E. Maggard, T. Nelson, M. Shaw, and J. P. Allebach, "Electrophotographic Ghosting Detection and Evaluation," in *Proceedings of NIP-31 IS&T's 2015 Conference on Digital Fabrication and Digital Printing*, (2015)
- [35] J. Wang, T. Nelson, R. Jessome, S. Astling, E. Maggard, M. Q. Shaw, and J. P. Allebach, "Local Defect Detection and Print Quality Assessment," *Image Quality and System Performance XIII*, IS&T Electronic Imaging, (2016)
- [36] Q. Chen, E. Maggard, R. Jessome, Y. Bang, M. Choi, and J. Allebach, "Segmentation-Based Detection of Local Defects on Printed Pages," in *Image Quality and System Performance XVI*, IS&T Electronic Imaging, (2019)
- [37] X. Xiang, E. Maggard, R. Jessome, Y. Bang, M. Choi, and J. Allebach, "Blockwise Detection of Local Defects on Printed Pages," *Image Quality and System Performance XVI*, IS&T Electronic Imaging, (2019)
- [38] H. S. Rosario, E. S., W. Wu, and K. Chandu, "Streak Detection in Mottled and Noisy Images," *Journal of Electronic Imaging*, vol. 16, no. 4, pp. 043005, (2007)
- [39] R. Zhang, E. Maggard, R. Jessome, Y. Bang, M. Choi, and J. Allebach, "Block Window Method with Logistic Regression Algorithm for Streak Detection," in *Image Quality and System Performance XVI*, IS&T Electronic Imaging, (2019)
- [40] O. A. Ugbeme, E. Saber, and W. Wu, "An automated Defect Classification Algorithm for Printed Documents," in *Proceedings of International Congress of Imaging Science*, pp 317-320, (2006)
- [41] O. A. Ugbeme, E. Saber, W. Wu, and K. Chandu, "Automated Algorithm for the Identification of Artifacts in Mottled and Noisy Images," *Journal of Electronic Imaging*, vol. 16, no. 3, pp 033015, (2007)
- [42] K. Chandu, E. Saber, and W. Wu, "A mutual Information Based Automatic Registration and Analysis Algorithm for Defect Identification in Printed Documents," in *2007 IEEE International Conference on Image Processing*, vol. 3, pp. III-449, (2007)
- [43] M. Q. Nguyen and J. P. Allebach, "Controlling Misses and False Alarms in a Machine Learning Framework," in *Image Quality and System Performance XII*, SPIE vol. 9396, (2015)
- [44] W. Wang, G. Overall, T. Riggs, R. Silveston-Keith, J. Whitney, G. T. C. Chiu, and J. P. Allebach, "Figure of Merit for Macrouniformity Based on Image Quality Ruler Evaluation and Machine Learning Framework," in *Image Quality and System Performance X*, SPIE vol. 8653, (2013)
- [45] W. Wang, Y. Guo, and J. P. Allebach, "Image Quality Evaluation Using Image Quality Ruler and Graphical Model," in *Proceedings of ICIP-2015 IEEE International Conference on Image Processing*, (2015)
- [46] Y. Yang, U. Sarkar, I. Borrell, and J. Allebach, "Ink quality ruler experiments and print uniformity predictor," in *Proceedings of Image Quality and System Performance XVII*, IS&T Electronic Imaging, (2020)
- [47] R. Zhang, Y. Yang, E. Maggard, Y. Bang, M. Choi, and J. Allebach, "A comprehensive system for analyzing the presence of print quality defects," in *Proceedings of Image Quality and System Performance XVII*, IS&T Electronic Imaging, (2020)
- [48] R. Zhang, E. Maggard, Y. Bang, M. Choi, and J. Allebach, "Region of interest extraction for image quality assessment," in *Proceedings of Image Quality and System Performance XVII*, IS&T Electronic Imaging, (2020)
- [49] J. C. Briggs, D. J. Forrest, A. H. Klein, and M. Tse, "Living with ISO-13660: Pleasures and Perils," in *NIP & Digital Fabrication Conference*, vol. 1999, no. 2, pp. 421-425, (1999)
- [50] ISO/IEC DIS 24790 International Standard, Information technology — Office equipment — Measurement of image quality attributes for hardcopy output — Monochrome text and graphic images, (2017)
- [51] ISO/IEC DIS 13660 International Standard, Information Technology — Office Equipment — Measurement of image quality attributes for hardcopy output — Binary monochrome test and graphic images, (2001).

- [52] D. Wolin, "Enhanced Mottle Measurement," in IS&T's 2002 PICS Conference, pages 148–151 (2002)
- [53] B. Streckel, B. Steuernagel, E. Falkenhagen, and E. Jung, "Objective Print Quality Measurements Using a Scanner and a Digital Camera," in IS&T International Conference on Digital Production Printing and Industrial Applications, pages 145–147, (2003)
- [54] K. He, G. Gkioxari, P. Dollár, and R. Girshick, "Mask RCNN," in Proceedings of the IEEE International Conference on Computer Vision, pages 2980-2988, (2017)
- [55] W. Xi, J. Chen, Q. Lin, and J. P. Allebach, "High-Accuracy Automatic Person Segmentation with Novel Spatial Saliency Map," in Proceedings of the IEEE International Conference on Image Processing, pages 1560-1564, (2019)
- [56] S. Ren, K. He, R. Girshick, and J. Sun, "Faster R-CNN: Towards Real-Time Object Detection with Region Proposal Networks," in Proceedings of the Advances in Neural Information Processing Systems, pages 91-99, (2015)
- [57] L. Bertinetto, J. Valmadre, J. F. Henriques, A. Vedaldi, and P. H. Torr, "Fully-Convolutional Siamese Networks for Object Tracking," in European Conference on Computer Vision, pages 850-865, (2016)
- [58] D. M. Montserrat, J. Chen, Q. Lin, J. P. Allebach, and E. J. Delp., "Multi-View Matching Network for 6D Pose Estimation," in IEEE International Conference on Computer Vision Workshops on 3D Scene Understanding for Vision, Graphics, and Robotics, (2019)
- [59] Y. Li, G. Wang, X. Ji, Y. Xiang, and D. Fox, "DeepIM: Deep Iterative Matching for 6D Pose Estimation," in Proceedings of the European Conference on Computer Vision, pages 683–698 (2018)
- [60] O. Russakovsky, J. Deng, H. Su, J. Krause, S. Satheesh, S. Ma, Z. Huang, A. Karpathy, A. Khosla, M. Bernstein, A. C. Berg, and F. Li, "Imagenet Large Scale Visual Recognition Challenge," International Journal of Computer Vision, 115(3), pages 211-252, (2015)
- [61] K. He, X. Zhang, S. Ren, and J. Sun, "Deep Residual Learning for Image Recognition," in Proceedings of the IEEE Conference on Computer Vision and Pattern Recognition, pages 770-778, (2016)
- [62] L. N. Smith, "Cyclical Learning Rates for Training Neural Networks," in IEEE Winter Conference on Applications of Computer Vision, pages 464-472, (2017)

## Author Biography

*Jianhang Chen is currently a Ph.D. candidate from Electrical and Computer Engineering, Purdue University. Before that, he joined NTU Robotics Lab and received his M.S. degree in Mechanical Engineering from National Taiwan University (2017). He received his B.S. in Info. and Comp. Science from Beihang University (2014). His research focuses on computer vision and deep learning, with emphasis on printed image quality and image registration.*

*Dr. Qian Lin is a research scientist working on computer vision and deep learning research in HP Labs. She is also an Adjunct Full Professor of Electrical and Computer Engineering, Purdue University. She received her BS from Xian Jiaotong University in China, her MSEE from Purdue University, and her Ph.D. in EE from Stanford University. Dr. Lin is the inventor/co-inventor for 44 issued patents. She was awarded Fellowship by the Society of IS&T in 2012, and Outstanding Electrical Engineer by the School of ECE of Purdue University in 2013. She was promoted to the rank of HP Fellow in 2019.*

*Jan P. Allebach received his B.S. from the University of Delaware in 1972, his M.S. from Princeton University in 1975 and his Ph.D. from Princeton University in 1976. He is now the Hewlett-Packard Distinguished Professor of Electrical and Computer Engineering at Purdue Uni-*

*versity. Allebach is a Fellow of the IEEE, the National Academy of Inventors, the Society for Imaging Science and Technology (IS&T), and SPIE. He was named Electronic Imaging Scientist of the Year by IS&T and SPIE, and was named Honorary Member of IS&T, the highest award that IS&T bestows. He has received the IEEE Daniel E. Noble Award, and is a member of the National Academy of Engineering. He recently served as an IEEE Signal Processing Society Distinguished Lecturer (2016-2017). His current research interests include image rendering, image quality, color imaging and color measurement, printer and sensor forensics, and digital publishing.*

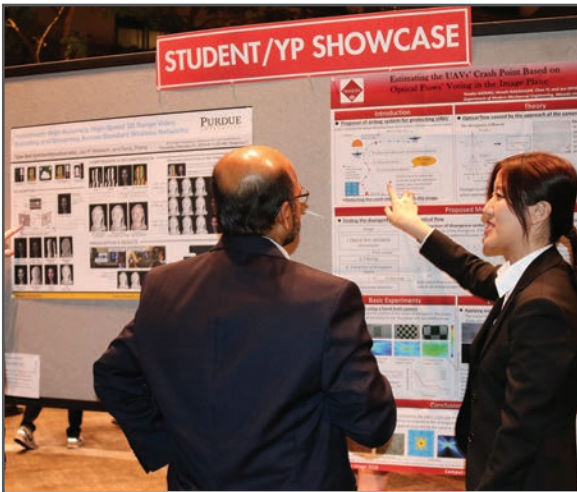
**JOIN US AT THE NEXT EI!**

IS&T International Symposium on

# Electronic Imaging

SCIENCE AND TECHNOLOGY

*Imaging across applications . . . Where industry and academia meet!*



- **SHORT COURSES • EXHIBITS • DEMONSTRATION SESSION • PLENARY TALKS •**
- **INTERACTIVE PAPER SESSION • SPECIAL EVENTS • TECHNICAL SESSIONS •**

[www.electronicimaging.org](http://www.electronicimaging.org)

